Investigation of numerical wall functions based on the 1D boundary layer equations for flows with significant pressure gradient

Tobias Knopp, Fabian Spallek, Octavian Frederich, and Gerd Rapin

Abstract In this paper we present a numerical wall function method for the simulation of isothermal flows with separation and reattachment based on the Reynolds averaged Navier-Stokes equations using an unstructured flow solver. The method is applied to the one-equation turbulence model by Spalart and Allmaras and is implemented in OpenFOAM®. For each wall node, a system of one-dimensional boundary-layer equations for the wall-parallel velocity component and for the turbulence quantity is integrated numerically on an embedded sub-grid in the near-wall region. The method is applied to the flow over a flat plate, over a backward facing step, and over a smoothly contoured ramp. The improvement of the results compared to universal wall functions become significant in case of separation and reattachment.

1 Introduction

Computational fluid dynamics (CFD) has become a mature tool for aerodynamic research and design optimization in automotive and aerospace research and industry. The statistically averaged (or: Reynolds averaged) Navier-Stokes (RANS) equations together with a one- or two-equation model of Spalart-Allmaras (SA) and k-ω type to model the mean effect of the turbulent stresses are a popular approach in CFD [3]. In order to obtain accurate numerical solutions, the thin boundary layers in the vicinity of viscous walls need to be captured by the computational grid. A so-called low-Re grid requires a spacing in viscous units of $y^+(1) \leq 1$ for the wall distance of the first node above the wall $y(1)$ and several grid nodes in the viscous sublayer. In

Tobias Knopp
DLR (German Aerospace Center), Institute of Aerodynamics and Flow Technology, Dept. $C^2A^2S^2E$, Bunsenstr. 10, 37073 Göttingen, Germany, e-mail: Tobias.Knopp@dlr.de

Fabian Spallek, Octavian Frederich, and Gerd Rapin
Volkswagen AG, 38436 Wolfsburg, Germany

the definition of $y^+(1) = y(1)u_\tau/\nu$, u_τ is the friction velocity and ν is the kinematic viscosity of the fluid. The requirements on low-Re grids cause several problems. The first is the large number of grid points to be placed into the boundary layers, which increases the computational costs significantly, especially for internal flows. The second (and most important) point is the challenge to generate proper low-Re meshes for complex geometries within a reasonable amount of time, in particular due to the high aspect ratios of the cells. The third issue is that the high aspect ratios of the grid cells near the wall increase the numerical stiffness and lead to a slower convergence of the solver. To illustrate typical problems in industrial CFD meshing, we show an example of collapsing boundary layers at the edges of a small gap on a car door in Figure 1 (left) and a boundary layer mesh on a car roof consisting of only a few number of layers of anisotropic hexa-cells in Figure 1 (right).

One solution strategy is to use wall-functions to bridge the near-wall region, see [3]. Then so-called high-Re meshes can be used with a first off-wall node at $y^+(1) \approx 50$ or larger. Albeit the basic idea is more than 40 years old, wall-functions are still a field of research. Standard wall-functions are based on the universal wall law, i.e., the log-law, which works quite successful in regions of attached, fully developed turbulent boundary layer flows without strong pressure gradients and without significant non-isothermal effects. Concerning the improvement of universal wall functions, an important step was the work by [5] on grid-independent hybrid universal wall functions, where the solution becomes (almost) independent of $y^+(1)$, provided that $y(1)$ is located in the log-layer or below. Such hybrid (or: adaptive) wall functions are based on the turbulence model specific near-wall solution of, e.g., the SA or the k-ω model.

In case of strong pressure gradients or non-isothermal effects, the near-wall solution can differ significantly from the universal wall-law. Then the idea is to increase the modelling complexity by including the dominant terms of the RANS equations into the near-wall model. For aerodynamic isothermal flows subjected to strong pressure gradients, the dominant terms are the pressure gradient and the mean inertial terms. The price to pay for this is that the arising (system of) equations can no longer be solved analytically but need to be integrated numerically. In [1], the two-dimensional boundary layer equations for the wall-parallel component of the velocity U and for the wall-normal velocity component V are solved on an embedded sub-grid in the vicinity of the viscous wall. However, the implementation of this method into an unstructured flow solver is not simple. Therefore the aim is to derive a system of one-dimensional boundary layer equations, which describes U and the turbulence quantities in wall-normal direction. Such a 1D method including the effects of the pressure gradient is considered in e.g. [11]. In [6] additionally the mean inertial terms are taken into account using an approximation, but the method is validated only for attached flows.

2 Governing equations and wall function modelling

We consider the stationary incompressible RANS equations for mean velocity $\mathbf{U}: \Omega \to \mathbb{R}^d$ and mean pressure $P: \Omega \to \mathbb{R}$ in a bounded, polyhedral domain $\Omega \subset \mathbb{R}^d$ ($d = 2,3$) with given source term $\mathbf{f} = \mathbf{0}$, kinematic viscosity ν and with the Reynolds stresses being modelled using the eddy-viscosity assumption

$$-\nabla \cdot (2(\nu + \nu_t)\mathbb{S}(\mathbf{U})) + \nabla \cdot (\mathbf{U} \otimes \mathbf{U}) + \nabla P = \mathbf{0} \qquad \text{in} \quad \Omega\,, \tag{1}$$

$$\nabla \cdot \mathbf{U} = 0 \qquad \text{in} \quad \Omega\,, \tag{2}$$

where $\mathbb{S}(\mathbf{u}) = \frac{1}{2}(\nabla \mathbf{u} + \nabla \mathbf{u}^T)$ is the rate of strain tensor. The eddy-viscosity $\nu_t = f_{v1}\tilde{\nu}$ is modelled using the Spalart-Allmaras one-equation turbulence model [10] which is formulated for $\tilde{\nu}$, and we seek $\tilde{\nu}: \Omega \to \mathbb{R}$ such that

$$\mathbf{U} \cdot \nabla \tilde{\nu} - \nabla \cdot \left(\frac{\nu + \tilde{\nu}}{\sigma} \nabla \tilde{\nu} \right) - \frac{c_{\mathrm{b2}}}{\sigma} \nabla \tilde{\nu} \cdot \nabla \tilde{\nu} = c_{\mathrm{b1}} \rho \tilde{S}(\mathbf{U}) \tilde{\nu} - c_{\mathrm{w1}} f_{\mathrm{w}} \left(\frac{\tilde{\nu}}{d} \right)^2 \quad \text{in} \quad \Omega\,, \tag{3}$$

where d is the distance to the closest wall. For the specification of f_{v1}, which is a function of $\tilde{\nu}/\nu$, $\tilde{S}(\mathbf{U})$, f_{w}, and the model constants c_{b1}, c_{b2}, c_{w1}, σ, we refer to [10]. Additionally, appropriate boundary conditions need to be specified. On the viscous wall Γ_{w}, we use $\mathbf{U} = \mathbf{0}$ and $\tilde{\nu} = 0$. On the inflow boundary we impose Dirichlet conditions for $\mathbf{U}$ and $\tilde{\nu}$. On the outflow boundary we prescribe homogeneous Neumann conditions for $\mathbf{U}$ and $\tilde{\nu}$.

Then we apply the wall-function concept. This can be interpreted as a domain-decomposition method with overlap [12]. Denote $\Omega_\delta \subset \Omega$ the near-wall region with an artificial inner boundary Γ_δ. We assume that $\mathrm{dist}(\Gamma_\delta, \Gamma_{\mathrm{w}}) \lessapprox 0.15\delta_{99}$, where δ_{99} denotes the boundary layer thickness [3]. We replace the problem (1)-(3) in Ω by two computationally less expensive problems:

- A *global flow* problem to be solved in the whole domain Ω with solution $\mathbf{U}: \Omega \to \mathbb{R}^d$, $P, \tilde{\nu}: \Omega \to \mathbb{R}$, and with modified boundary condition for $\mathbf{U}$ on Γ_{w}.
- A *boundary-layer problem* to be solved for the wall-parallel velocity component $U: \Omega_\delta \to \mathbb{R}$, and for $\tilde{\nu}^{\mathrm{bl}}: \Omega_\delta \to \mathbb{R}$.

Then the *wall-function formulation* reads as follows:

Global RANS problem. Solve (1)-(3) in Ω with modified boundary condition

$$\mathbf{u} \cdot \mathbf{n} = 0, \quad (\mathbb{I} - \mathbf{n} \otimes \mathbf{n}) 2\nu \mathbb{S}(\mathbf{U})\mathbf{n} = -\tau_{\mathrm{w}}^{\mathrm{bl}} \hat{\mathbf{U}}_{\mathrm{t},\delta} \quad \text{on} \quad \Gamma_{\mathrm{w}}. \tag{4}$$

Therein $\mathbf{n}$ is the unit surface normal vector and $\mathbb{I} - \mathbf{n} \otimes \mathbf{n}$ is the projection operator onto the tangential space of Γ_{w}. Moreover we introduce $\hat{\mathbf{U}}_{\mathrm{t},\delta} = \mathbf{V}_{\mathrm{t},\delta}/|\mathbf{V}_{\mathrm{t},\delta}|$ with $\mathbf{V}_{\mathrm{t},\delta} = (\mathbb{I} - \mathbf{n} \otimes \mathbf{n})\,\mathbf{U}|_{\Gamma_\delta}$ and $U_\delta \equiv |\mathbf{V}_{t,\delta}|$.

Near-wall problem. For each $\mathbf{x}_{\mathrm{w}} \in \Gamma_{\mathrm{w}}$ we solve a 1D boundary value problem along the wall-normal line $\{\, \mathbf{x}_{\mathrm{w}} - y\mathbf{n} \mid y \in (0, y_\delta) \}$ where $y_\delta \equiv \mathrm{dist}(\Gamma_\delta, \Gamma_{\mathrm{w}})$, which is derived from (1)-(3) using boundary layer theory, see, e.g. [8]:

$$-\frac{\mathrm{d}}{\mathrm{d}y}\left((\nu+\nu_{\mathrm{t}}^{\mathrm{bl}})\frac{\mathrm{d}U^{\mathrm{bl}}}{\mathrm{d}y}\right)=f\,, \tag{5}$$

$$-\frac{\mathrm{d}}{\mathrm{d}y}\left(\frac{\nu+\tilde{\nu}^{\mathrm{bl}}}{\sigma}\frac{\mathrm{d}\tilde{\nu}^{\mathrm{bl}}}{\mathrm{d}y}\right)=\frac{c_{\mathrm{b2}}}{\sigma}\left(\frac{\mathrm{d}\tilde{\nu}^{\mathrm{bl}}}{\mathrm{d}y}\right)^2+c_{\mathrm{b1}}\rho\tilde{S}^{\mathrm{bl}}\tilde{\nu}^{\mathrm{bl}}-c_{\mathrm{w1}}f_{\mathrm{w}}\left(\frac{\tilde{\nu}^{\mathrm{bl}}}{y}\right)^2. \tag{6}$$

Therein $\nu_{\mathrm{t}}^{\mathrm{bl}}=f_{v1}^{\mathrm{bl}}\tilde{\nu}^{\mathrm{bl}}$, where f_{v1}^{bl} is a function of $\tilde{\nu}^{\mathrm{bl}}/\nu$. The boundary conditions for U^{bl} and $\tilde{\nu}^{\mathrm{bl}}$ impose the no-slip condition on Γ_w and ensure matching with the global solution on Γ_δ

$$U^{\mathrm{bl}}=0\,,\ \tilde{\nu}^{\mathrm{bl}}=0\quad\text{for } y=0\,,\qquad U^{\mathrm{bl}}=U_\delta\,,\ \tilde{\nu}^{\mathrm{bl}}=\tilde{\nu}_\delta\equiv\tilde{\nu}|_{\Gamma_\delta}\quad\text{for } y=y_\delta\,. \tag{7}$$

Finally, from U^{bl} the wall-shear stress τ_w^{bl} is computed

$$\tau_w^{\mathrm{bl}}=\nu\frac{\mathrm{d}U^{\mathrm{bl}}}{\mathrm{d}y}|_{y=0} \tag{8}$$

and can be provided as boundary condition for the global flow problem in (4). The right hand side f in (5) can be computed using different levels of complexity

$$f=\begin{cases}0 & \text{: stress-equilibrium,}\\ -\frac{1}{\rho}\frac{\mathrm{d}P}{\mathrm{d}x} & \text{: pressure gradient,}\\ -\frac{1}{\rho}\frac{\mathrm{d}P}{\mathrm{d}x}-U^{\mathrm{bl}}\frac{\partial U^{\mathrm{bl}}}{\partial x}-V^{\mathrm{bl}}\frac{\partial U^{\mathrm{bl}}}{\partial y} & \text{: full approximation.}\end{cases} \tag{9}$$

We add some remarks on the 1D problem (5), (6). Firstly, it is formulated in a wall-fitted coordinate system with x being the streamwise direction and y being the wall-normal direction, and U^{bl} and V^{bl} are the wall-parallel and the wall-normal component of the mean velocity. Secondly, using boundary layer theory [8] we assume that $\mathrm{d}P^{\mathrm{bl}}/\mathrm{d}x=\mathrm{d}P/\mathrm{d}x$ at least in the inner part of the boundary layer. Thirdly, we come to the most important aspect. The option using the full approximation in (9) is unclosed. The quantity $\partial U^{\mathrm{bl}}/\partial x$ is not known as a function of y in a 1D approach. Instead, $\partial U^{\mathrm{bl}}/\partial x$ is known only at $y=0$ and at $y=y_\delta$ from the global problem. The quantity V is also not known in (5) in $(0,y_\delta)$. Therefore the sum convective term requires closure modelling. Following [13], $U\partial U/\partial x+V\partial U/\partial y$ can be expressed in terms of $U(y)$ and $\mathrm{d}u_\tau/\mathrm{d}x$. This is seen as a motivation to consider the following two approximations based on U^{bl}

$$U^{\mathrm{bl}}\frac{\partial U^{\mathrm{bl}}}{\partial x}+V^{\mathrm{bl}}\frac{\partial U^{\mathrm{bl}}}{\partial y}\approx\begin{cases}U^{\mathrm{bl}}\frac{\partial U_\delta}{\partial x}\frac{U^{\mathrm{bl}}}{U_\delta} & \text{: quadratic approx. in } U^{\mathrm{bl}}\,,\\ U^{\mathrm{bl}}\frac{\partial U_\delta}{\partial x}\frac{y}{y_\delta} & \text{: linear approx. in } U^{\mathrm{bl}}\,.\end{cases} \tag{10}$$

These approximations for the sum convective term will be discussed in Section 4.2.

3 Numerical solution method using OpenFOAM®

For the numerical simulations, OpenFOAM®is used. This is an unstructured finite volume solver on collocated meshes. The method is of cell-centered type, i.e., the flow variables are assigned to the centroids of the control volumes. For the momentum equation, the convective fluxes are discretized using a linear upwind scheme in our study. The diffusive fluxes are discretized with a central scheme, i.e., the gradients are reconstructed using the Green-Gauss formula in conjunction with a gradient correction for non-orthogonal cells. The momentum and continuity equations are coupled regarding velocity and pressure. They are solved iteratively using a projection method, viz., the SIMPLE method. The corresponding iterations are called outer iterations. For the outer iteration loop, we use under-relaxation with relaxation factors $\alpha_p = 0.3$ for p, $\alpha_u = 0.7$ for U and $\alpha_{\tilde{\nu}} = 0.7$ for $\tilde{\nu}$. As the values of velocity and pressure are computed on the same set of nodes, a variant of the interpolation scheme by Rhie and Chow is applied, see [4]. For the solution of the arising linear systems we use a preconditioned bi-conjugate gradient solver (PBiCG) for asymmetric matrices together with diagonal incomplete LU (DILU) preconditioning for the momentum and turbulence model equations. For solving the pressure equation, we use a generalised geometric-algebraic multi-grid solver (GAMG) with a smoothing method of Gauss-Seidel type.

Within each outer iteration step of the SIMPLE method, the near-wall problem (5)-(7) is solved on an embedded sub-grid using a second order accurate finite difference scheme, see Figure 2. The arising linear systems for wall-parallel velocity and for $\tilde{\nu}$ are tri-diagonal and are solved directly using the Thomas-algorithm. Then we determine τ_w^{bl} using (8) and compute $u_\tau^{\mathrm{bl}} = \sqrt{\tau_w^{\mathrm{bl}}/\rho}$. As an implementation detail, the right hand side of (4) is not directly used but is altered, which is typical to cell-centered schemes. Firstly, in (8) the underresolved mean velocity gradient on the global mesh is used. Secondly, ν is replaced by $\nu + \nu_{\mathrm{t,WF}}$ in order to obtain the correct τ_w^{bl}. This is achieved by defining

$$\nu_{\mathrm{t,WF}} = \nu \max\left(1, \frac{y_\delta^+}{U^{\mathrm{bl},+}(y_\delta^+)}\right), \quad U^{\mathrm{bl},+} = \frac{U^{\mathrm{bl}}}{u_\tau^{\mathrm{bl}}}, \quad y_\delta^+ = \frac{y_\delta u_\tau^{\mathrm{bl}}}{\nu}. \tag{11}$$

4 Results

4.1 Turbulent boundary layer flow at zero pressure gradient

The method is applied first to a turbulent boundary layer flow at zero pressure gradient (ZPG). We consider the flow over a flat plate of length $l = 5\mathrm{m}$ at inflow velocity $u_\infty = 33\mathrm{ms}^{-1}$ and $\nu = 1.51 \times 10^{-5}\mathrm{m}^2\mathrm{s}^{-1}$. The wall is treated fully turbulent.

For zero pressure gradient flows, corresponding to $f = 0$ in (9), the deviation to the low-Re solution should be very similar between the Spalding wall-function

and the numerical wall-function. We generate a series of meshes using the same distribution function for the grid points in wall-normal direction, where the wall-distance of the first node $y(1)$ and hence the number of mesh points are varied. The aim is to obtain results which are robust w.r.t. changes in $y^+(1)$. We consider high Re meshes with $y^+(1) = 65$ and $y^+(1) = 160$. The number of nodes in wall-normal direction inside the boundary layer, i.e., with wall distance $y < \delta_{99}$, is 190 for the low-Re mesh but only 24 on the mesh with $y^+(1) = 65$.

The results for the skin friction coefficient $c_f = 2(u_\tau/u_\infty)^2$ using numerical wall functions (num WF) and universal wall functions using the wall law by Spalding (Spalding) are shown in Figure 2. The deviation from the low-Re solution for $x > 3$m is similar for the Spalding wall function and for the numerical wall function on the mesh with $y^+(1) = 65$, but the deviation for the numerical wall function becomes larger on the mesh with $y^+(1) = 160$.

4.2 Flow over a smoothly contoured ramp

In this section we consider the flow by [9], where separation is caused by an adverse pressure gradient on a smoothly contoured surface. In the simulation, a turbulent boundary layer develops over a long flat plate of length 2.0m and then follows the smoothly contoured ramp of length 70mm and height $h = 21$mm, see also [7]. Due to the ramp the flow experiences an adverse pressure gradient, causing the boundary layer to separate, and the flow reattaches on the downstream flat plate. The ramp starts at $x = 0$ and ends at $x = 70\text{mm} = 3.33h$. The flow conditions are given at the reference position $x_{\text{ref}} = -140$mm. We consider the cases $Re_\theta = 3400$ and $Re_\theta = 20100$. For $Re_\theta = 3400$, the boundary layer edge velocity is $U_\text{e} = 20.2\text{ms}^{-1}$, $\delta_{99} = 27.6$mm and $\nu = 15.5 \times 10^{-5}\text{m}^2\text{s}^{-1}$. For $Re_\theta = 20100$, the data are $U_\text{e} = 20.5\text{ms}^{-1}$, $\delta_{99} = 26.0$mm and $\nu = 2.06 \times 10^{-6}\text{m}^2\text{s}^{-1}$.

For $Re_\theta = 20100$, we study the boundary layer approximation and consider the order of magnitude of the terms in (9). Moreover we assess the approximations in (10). We extract the profiles for $\mathrm{d}P/\mathrm{d}x$, $U\partial U/\partial x$ and $V\partial U/\partial y$ along a wall-normal line at $x = 35$mm in the mid of the ramp in the adverse pressure gradient region. We scale the terms in (9) to inner units by multiplication with $\nu/(\rho u_\tau^3)$. Figure 3 (left) shows the results. The term $\mathrm{d}P/\mathrm{d}x$ is almost constant in wall-normal direction, and the deviation from the constant behaviour is due to the surface curvature of the ramp [8]. The term $U\partial U/\partial x$ is significantly larger than $V\partial U/\partial y$, but the latter term is not negligible small. Note that in a decelerating boundary layer typically $\partial U/\partial x$ is negative, whereas U, V, and $\partial U/\partial y$ are positive. Therefore $V\partial U/\partial y$ reduces $U\partial U/\partial x$. For $y^+ \gtrapprox 50$, the total convective term is of the same order of magnitude as $\mathrm{d}P/\mathrm{d}x$. In Figure 3 (right) the two approximations to $U\partial U/\partial x + V\partial U/\partial y$ proposed in (10) are assessed. Since both V and $\partial U/\partial y$ are not known accurately on Γ_δ, the contribution of $V\partial U/\partial y$ is neglected. This leads to an overestimation of the total mean convection term by around 15% to 20%. The approximations given in (10) are shown for two different positions of Γ_δ, i.e., at $y_\delta^+ = 50$, and 100. The

quadratic approximation gives a qualitatively close approximation and is superior to the linear approximation. However, in some circumstances, e.g., near separation and reattachment, the linear approximation has better numerical properties than the quadratic approximation, as described in the next paragraph.

The predictions for c_f are shown in Figure 4 for a mesh with $y^+(1) = 30$ at the reference position. Note that the reference solution is the low-Re solution, not the experimental data. The numerical wall functions are applied using the second and third approximation for f in (9). For the mean convective term we use the linear and the quadratic approximation in (10). The local peak of c_f at $x = 0$ due to the local flow acceleration is captured quite well using the numerical wall functions. Moreover, the flow deceleration in the adverse pressure gradient region on the ramp and the decrease in c_f are predicted in close agreement with the low-Re solution. The prediction in the separation region and after reattachment is also closer to the low-Re solution than for the Spalding wall functions. Note that the spurious oscillations in c_f at $x \approx 0.07m$ are caused by the kink in the geometry, which causes mild oscillations in $\mathrm{d}P/\mathrm{d}x$. In the vicinity of separation and reattachment, the solution using the quadratic approximation suffers from additional oscillations, which are not observed for the linear approximation. Finally we mention that regarding the performance acceleration of the method, wall functions give a speed up of a factor of more than three regarding the solver iterations compared to the low-Re mesh.

4.3 Flow over a backward facing step

In this section we consider the turbulent flow over a long flat plate, where sudden flow separation is caused by a backward-facing step of height h at $x = 0$, followed by reattachment at $x/h = 6.26 \pm 0.10$. The channel height upstream of the step is $8h$ and the length of the inflow section is $110h$. The test case was studied experimentally by Driver and Seegmiller [2]. In agreement with the experimental flow conditions, the inflow centerline velocity prior to the step is $U_0 = 44.2\mathrm{ms}^{-1}$, the Reynolds number based on the momentum thickness [3] is $Re_\theta \approx 5000$ and the boundary layer thickness is $\delta_{99} \approx 1.5h$. The height of the step is $h = 0.0127$m, yielding $Re_h = U_0 h/\nu \approx 36000$. Wall-functions are used on the top and bottom wall. The wall opposite the step was parallel to the wall in the experiment considered here. On the low-Re mesh, the number of grid points in wall-normal direction with wall distance $y < \delta_{99}$ is 102, whereas on the high-Re mesh with $y^+(1) = 55$ (measured at $x/h = -2$) only 20 points are needed.

The results are shown in Figure 5. The predictions using numerical wall functions are significantly closer to the low-Re solution than for the Spalding wall function. The deviation with and without the convective term are very small.

5 Conclusion

We presented a numerical wall function method for aerodynamic flows with separation and reattachment applied to the Spalart-Allmaras (SA) model. The wall function method is implemented and validated using the unstructured incompressible flow solver OpenFOAM®. The method solves a one-dimensional boundary layer equation for the wall-parallel velocity and for the SA model on an embedded subgrid in the near-wall region. For a robust usage of the present method for complex configurations, meshes with $y^+(1) = 30$ seem to be a good compromise between robustness and accuracy of the method. On meshes with $y^+(1) = 30$, the pressure gradient term is the most important term in the boundary layer equations. Taking into account additionally the mean convection term does not give significant improvements in accuracy for the test cases and meshes studied in this work, but is found to degrade the robustness of the method.

Acknowledgements The authors are grateful to Profs. Rossow and Radespiel and to Dr. Sundermeier for valuable discussions and to Prof. Eaton for providing the experimental data.

References

1. T. J. Craft, S. E. Gant, H. Iacovides, and B. E. Launder. Development and application of a new wall function for complex turbulent flows. In *Proceedings of the European Conference on Computational Fluid Dynamics (ECCOMAS CFD 2001)*, 2001.
2. D. M. Driver and H. L. Seegmiller. Features of a reattaching turbulent shear layer in divergent channel flow. *AIAA Journal*, 23(2), 1985.
3. P. A. Durbin and B. A. Petterson Reif. *Statistical theory and modelling for turbulent flows*. John Wiley & Sons, Chichester, 2001.
4. H. Jasak. *Error analysis and estimation for the finite volume method with applications to fluid flows*. PhD thesis, Imperial Collegue London, 1996.
5. G. Kalitzin, G. Medic, G. Iaccarino, and P. Durbin. Near-wall behaviour of RANS turbulence models and implications for wall functions. *Journal of Computational Physics*, 204:265–291, 2005.
6. T. Knopp. Improved wall functions based on the 1d boundary layer equations for flows with significant pressure gradient. In *New Results in Numerical and Experimental Fluid Mechanics VII. Contributions to the 16th STAB/DGLR Symposium Aachen, Germany 2008*, 2008.
7. G. Medic, G. Kalitzin, G. Iaccarino, and E. van der Weide. Adaptive wall functions with applications. *AIAA Paper 2006-3744*, 2005.
8. H. Schlichting. *Boundary-Layer Theory*. McGraw-Hill, New York, 1979.
9. S. Song and J. K. Eaton. Reynolds number effects on a turbulent boundary layer with separation, reattachment and recovery. *Experiments in Fluids*, 36:246–258, 2004.
10. P. R. Spalart and S. R. Allmaras. A one-equation turbulence model for aerodynamics flows. *AIAA Paper 1992-0439*, 1992.
11. F. Tessicini, L. Temmerman, and M. Leschziner. Approximate near-wall treatments based on zonal and hybrid RANS-LES methods for LES at high Reynolds numbers. *International Journal of Heat and Fluid Flow*, 27:789–799, 2006.
12. M. D. Tidriri. Domain decomposition for compressible Navier-Stokes equations with different discretizations and formulations. *Journal of Computational Physics*, 119:271–282, 1995.

13. B. van den Berg. A three-dimensional law of the wall for turbulent shear flows. *Journal of Fluid Mechanics*, 70:149–160, 1975.

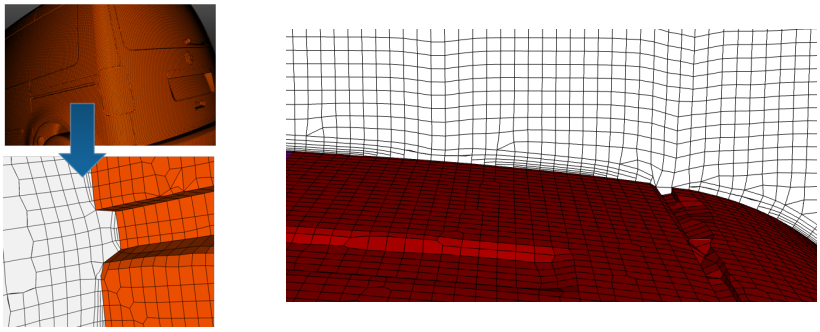

Fig. 1 Example of typical problems in industrial CFD meshing. Left: Collapsing boundary layers at the edges of a small gap on a door. Right: Boundary layer mesh on the car roof consisting of six or less layers of anisotropic hexa-cells. Isotropic hexa-cells are used outside of the boundary layer.

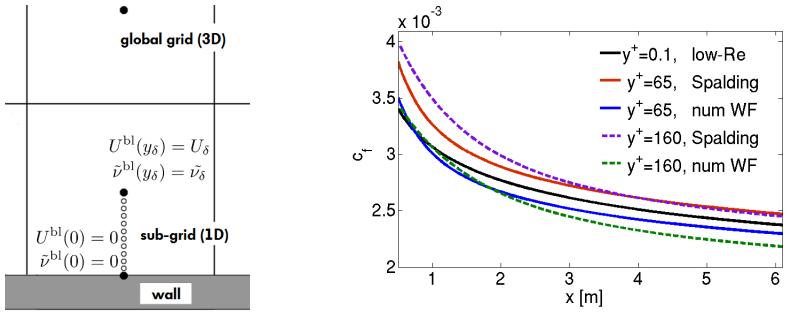

Fig. 2 Left: Sketch of the embedded sub-grid for solving the 1D boundary layer equations. Right: Turbulent boundary layer flow over a flat plate at zero pressure gradient. Distribution of the skin friction coefficient c_f using wall functions on high-Re grids compared to the low-Re solution.

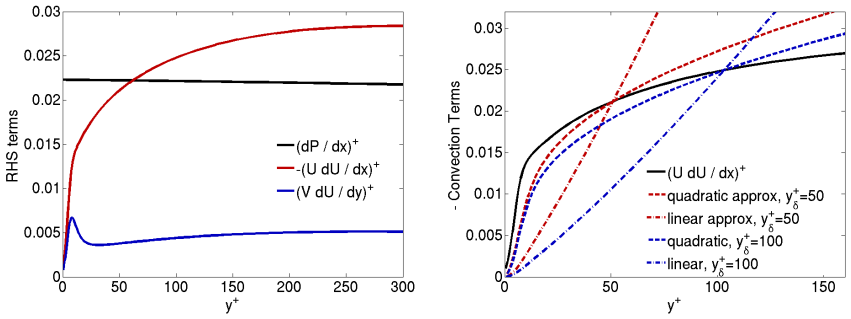

Fig. 3 Flow over a smoothly contoured ramp at $Re_\theta = 20100$ [9]. Left: Right hand side (RHS) terms extracted from the low-Re solution in the mid of the ramp at $x = +35$mm in the adverse pressure gradient region along a wall-normal line. Right: Approximation of the convective term in (10). Note that the convection terms are plotted with a minus sign in the right figure.

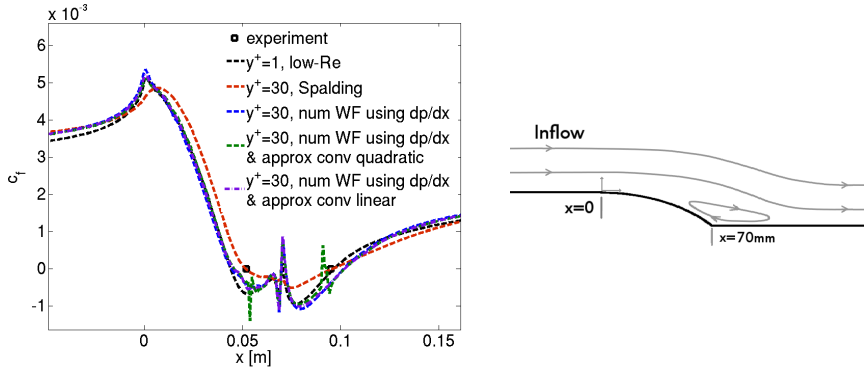

Fig. 4 Smoothly contoured ramp at $Re_\theta = 3400$: Distribution of friction coefficient c_f for high-Re grid and different wall functions compared to low-Re solution (left) and sketch of the flow (right).

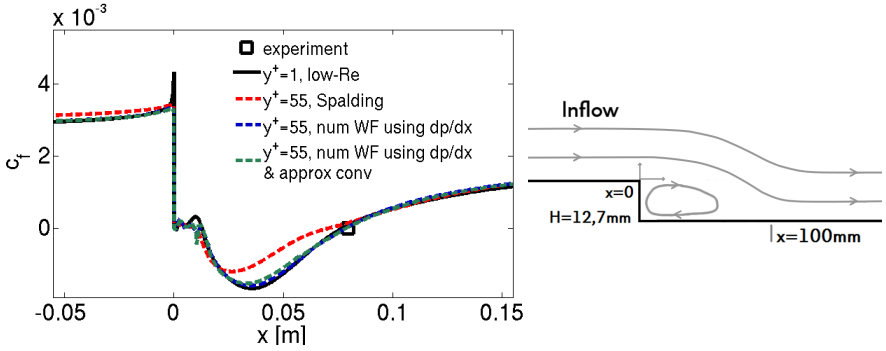

Fig. 5 Flow over a backward facing step [2]: Distribution of friction coefficient c_f for high-Re grid and different wall functions compared to low-Re solution (left) and sketch of the flow (right).